

Scaling Methods To Estimate Macroscopic Fundamental Diagrams in Urban Networks with Sparse Sensor Coverage

Nandan Maiti^a, Manon Seppacher^a, Ludovic Leclercq^a

^a*Univ. Eiffel, ENTPE, LICIT-ECO7, Lyon, 69500, France*

Abstract

Accurately estimating traffic variables across unequipped portions of a network remains a significant challenge due to the limited coverage of sensor-equipped links, such as loop detectors and probe vehicles. A common approach is to apply uniform scaling, treating unequipped links as equivalent to equipped ones. This study introduces a novel framework to improve traffic variable estimation by integrating statistical scaling methods with geospatial imputation techniques. Two main approaches are proposed: (1) Statistical Scaling, which includes hierarchical and non-hierarchical network approaches, and (2) Geospatial Imputation, based on variogram modeling. The hierarchical scaling method categorizes the network into several levels according to spatial and functional characteristics, applying tailored scaling factors to each category. In contrast, the non-hierarchical method uses a uniform scaling factor across all links, ignoring network heterogeneity. The variogram-based geospatial imputation leverages spatial correlations to estimate traffic variables for unequipped links, capturing spatial dependencies in urban road networks. Validation results indicate that the hierarchical scaling approach provides the most accurate estimates, achieving reliable performance even with as low as 5% uniform detector coverage. Although the variogram-based method yields strong results, it is slightly less effective than the hierarchical scaling approach but outperforms the non-hierarchical method.

Keywords: Network scaling, Macroscopic fundamental diagrams, Spatial imputation, Loop detectors, Equipped networks.

1. Introduction

The Macroscopic Fundamental Diagram (MFD) has emerged as a critical tool in network traffic management, providing a relationship between aggregate traffic variables such as flow, density, and speed across an entire urban road network [1]. This concept offers valuable insights for network traffic control [2, 3], particularly in perimeter control strategies [4, 5, 6], where traffic inflow and outflow are managed to optimize network-wide performance. By monitoring traffic at a macroscopic level, the MFD enables decision-makers to regulate traffic in real-time, improve congestion management, and enhance the overall efficiency of urban transportation systems.

Despite its potential, estimating a reliable MFD for a city network requires extensive empirical data. Loop detector device (LDD), the most commonly used data source for MFD estimation, collects information from fixed sensors embedded in road infrastructure [7, 8, 9, 10, 4, 11, 12, 13, 14]. However, LDD faces limitations, such as positional biases in speed estimation, as well as the inability to install sensors on all network links, leading to incomplete coverage [13]. To address these limitations, floating car device (FCD), or Probe Vehicle Data, is often used in combination with LDD [15, 16, 17, 18, 19, 20, 21, 22, 23, 24, 25, 26, 27]. FCD, derived from GPS-enabled vehicles, can capture vehicle trajectories and speeds, reducing the positional bias inherent in LDD. However, FCD has its own challenges, including the uncertain penetration rate of vehicles equipped with GPS in time and space. Estimating network-wide traffic flows based on the assumption of homogeneous FCD penetration introduces uncertainty in the flow estimation, particularly when coverage is sparse [28, 29, 30].

The limitations of these data sources underscore a broader issue: the network-wide traffic data used for MFD estimation is typically incomplete. LDD and FCD are often available only for certain links in the network, resulting in what is known as an ‘equipped network MFD’, an MFD that only reflects the links where sensors or FCD are deployed [26]. Consequently, this equipped MFD may not be representative of the entire network. Estimating an accurate MFD for the entire city remains challenging due to the spatial coverage limitations of available data.

To scale the equipped network MFD to the full city network, previous studies have attempted to partition the network into homogeneous areas and apply a scaling factor that adjusts for the ratio between the total length of links in the network and the length of the equipped links [26]. While this

approach can offer some level of approximation, it suffers from significant limitations. The partitioning of the network based on equipped network data can lead to erroneous estimations of homogeneous areas, as the unequipped links may exhibit different traffic characteristics [31, 6, 23, 32, 33, 34]. Furthermore, applying a uniform scaling factor across areas with varying types of links, such as arterials and local roads, results in inaccurate flow estimates.

Recent research has recognized the need for a more nuanced approach to spatial scaling of the MFD. To overcome the challenges associated with uniform scaling, a new methodology that accounts for the link hierarchy within a network is required. This method involves developing separate scaling factors for different hierarchical levels of the network, such as major arterials, collectors, and local streets. By accounting for the differences in traffic behavior at various link levels, this approach offers a more accurate estimation of network flow variables, allowing for the scaling of MFD from sensor-equipped portions of the network to the entire city.

This study proposes a comprehensive framework for spatial scaling of MFD that bridges the gap between sensor-equipped networks and the full urban road network. By incorporating link-hierarchical scaling and addressing the limitations of existing partitioning methods, we aim to improve the accuracy of network-wide MFD estimation, paving the way for more effective traffic management and control strategies at the city level.

1.1. Literature Review

1.1.1. Equipped Network

The literature about MFD estimation from ‘equipped network’ to ‘full network’ can be broadly classified into two groups based on the data used: one using empirical data sources from the equipped network, the other relying on large-scale simulation frameworks for a city. The main challenges associated with the empirical data are the limited coverage of LDD and FCD throughout the network, and the simulation fails to replicate the network topology and link hierarchy of a complex network [28, 27]. Therefore, including simulation data can only ensure, to a specific extent, an understanding of the hierarchical links and their characteristics on estimation average network flow variables. Thus, we mainly focused on the existing empirical study on MFD estimation and calibration.

MFD estimation predominantly relied on LDD [15, 7] information on vehicle counts and occupancy rates on road segments, allowing the calculation of network-wide average flow and density. This approach was inspired by

EDIE [35] definition of traffic flow metrics, where average flow and density are calculated based on the data collected from multiple equipped links within a network [28]. However, the reliance on LDD has certain limitations. For example, LDD is an Eulerian observation method, which may introduce bias in MFD estimation, particularly due to the spatial distribution of detectors [28]. The placement of detectors, often in congested areas or near traffic signals, can result in an overestimation of network density and contribute to scatter in the MFD [11]. However, a key challenge arises when MFD is estimated from LDD with only a subset of network links equipped with detectors. In such cases, the derived MFD reflects the equipped sub-network rather than the entire network [36, 26]. Despite this limitation, studies have shown that MFDs derived from a small fraction of links can still approximate critical density ranges observed in the full network MFD [11]. Mariotte et al. [26] introduced the concept of an ‘active network’ to improve MFD estimation, focusing on major arterials and secondary roads. They highlighted the importance of scaling the production MFD based on the ratio of total network length to equipped network length. The estimated scaling factor for production is based on the assumption of homogeneous network partitioning [37, 23, 32, 31, 34] using the equipped network information, leading to ambiguity in portioning for full network. Saffari et al. [38] expanded on this by investigating the selection of critical links for MFD estimation, though they noted that their findings were sensitive to the specific test bed used.

1.1.2. Spatial Scaling

The main challenge with imputing traffic states at the unequipped links is the estimation errors due lack of available information from the surrounding links. Network traffic state estimation approaches can be broadly classified into two main categories: model-driven and data-driven [39, 40]. High-accuracy model-driven methods often require additional information, such as detailed traffic signal settings or individual vehicle detector actuation data [41, 28]. While these methods have proven efficient in estimating traffic states, particularly at the link level [42, 43], their accuracy is highly dependent on the quality of the embedded models. Data-driven approaches leverage large amounts of historical data to train models using machine learning or statistical techniques [44, 45, 46, 40]. Since data-driven methods do not rely on strict theoretical assumptions, the accuracy of the models is largely influenced by the quantity and quality of the data. However, missing data is a common issue in data-driven methods, and several studies have attempted

to address this problem [47, 48, 49]. Nowadays, graph convolution networks (GCN), generative adversarial networks (GANs), and physics-informed neural networks (PINNs) are gaining significant attention in estimating the missing traffic flow variables in unequipped networks. GCNs struggle with capturing dynamic temporal changes in traffic networks, as they are often designed for static graphs. Additionally, the hierarchical and complex topology of traffic networks complicates model training [50, 51, 52, 53, 54]. GANs face difficulties generating realistic traffic data due to the stochastic nature of traffic demand, making adversarial training unstable [55, 56]. PINNs, while incorporating physical laws, may struggle with noisy or incomplete data, as real-world traffic patterns can deviate significantly from theoretical models [57, 58]. Balancing accuracy and computational efficiency remains a significant challenge across these approaches.

1.1.3. Geo-spatial scaling

In transportation data, kriging has been used to impute missing values in Annual Average Daily Traffic (AADT) datasets, with studies showing its superiority over traditional regression models like ordinary least squares (OLS) [59, 60]. The kriging method outperformed OLS, particularly in regions with moderate-to-high traffic volumes. However, under low traffic flow conditions, it tends to overestimate the missing data [60]. One of the limitations of the Kriging method is its reliance on Euclidean distance, which may not be ideal for transportation networks where distances are more appropriately measured along road networks. Zou et al. [61] proposed the use of an approximated road network distance based on isometric embedding theory to address this issue, improving the interpolation accuracy, particularly in complex road networks. Nevertheless, studies such as Selby and Kockelman [62] indicated that the use of road network distances does not always significantly improve prediction performance compared to traditional Euclidean distance-based methods.

In addition, while kriging has demonstrated success in spatial imputation, its application to spatio-temporal data remains relatively underexplored. Some studies, such as those by Yang et al. [63], have extended kriging to account for both spatial and temporal dimensions. These efforts aim to better capture the spatio-temporal characteristics of traffic data. Moreover, Marcotte [64] proposed cokriging, which uses secondary correlated variables alongside the primary variable, has shown promise in various fields. The application of cokriging for traffic data imputation is an area worth exploring,

especially given the availability of multiple sources of traffic data [65]. A recent study by Bae et al. [66] proposed the use of spatiotemporal cokriging to impute missing traffic flow speed data, integrating multiple data sources. Their results demonstrate that spatiotemporal cokriging improves the accuracy of imputation, particularly when missing data exhibit non-random patterns, such as blocks of missing data, which occur due to system malfunctions or maintenance issues. Later, Laval [67] showed that the traffic flow variables such as travel times, relaxation times, and delay in urban networks near critical density follow the scaling with total network length.

Despite the advancements in using the MFD for traffic management, several gaps remain. Current methods rely on incomplete data from LDD and FCD, leading to inaccurate MFD estimates that don't fully represent the entire network. Uniform scaling approaches overlook the hierarchical nature of urban road networks, resulting in imprecise flow and density estimates across different road types. Additionally, advanced data-driven models like GCNs and PINNs struggle with missing or noisy data, limiting their effectiveness in estimating traffic states. Moreover, traditional spatial scaling techniques such as kriging are not well-explored for complex road networks. A more refined approach, incorporating link-hierarchical scaling and better data imputation, is needed to improve MFD accuracy for complete network estimation.

2. Objectives and Contributions

Estimating a reliable MFD for an entire urban network remains a significant challenge due to the incomplete and biased coverage of traditional data sources like LDD and FCD. Existing methods often rely on uniform scaling approaches or oversimplified assumptions, which fail to capture the spatial and hierarchical variability of urban networks. These limitations hinder the accurate estimation of traffic flow dynamics across different road types, particularly in unequipped parts of the network, leading to suboptimal traffic management and control strategies. To address these challenges, this study develops a comprehensive framework for scaling network flow dynamics from equipped to full networks by incorporating road hierarchy and geospatial techniques.

1. The primary contributions of this work include a novel hierarchical statistical scaling framework, which accounts for the distinct traffic

characteristics of different road types, such as arterials and local streets, overcoming the inaccuracies of uniform scaling methods.

2. Adapts geospatial interpolation methods such as spatiotemporal variogram for traffic flow data, leveraging secondary data sources to address gaps and inconsistencies in LDD/FCD coverage and accurate estimation of network traffic dynamic.
3. Provides a robust evaluation of the proposed methodologies using real-world traffic data, demonstrating their effectiveness in capturing network-wide flow dynamics.

By addressing key challenges in spatial scaling, this study advances the state-of-the-art in MFD estimation, contributing to more efficient urban traffic management systems.

3. Methodology

The proposed methodology estimates traffic variables for an entire network based on partially sensor-equipped data using statistical scaling and geospatial imputation approaches. Initially, the network is classified into equipped and unequipped links. The statistical approach includes hierarchical and non-hierarchical scaling. In the hierarchical method, links are categorized into several levels based on spatial and functional characteristics (in this study: Hierarchy-1, Hierarchy-2, and Hierarchy-3), with tailored scaling factors applied to estimate traffic on unequipped links. The non-hierarchical method applies uniform scaling across all links. The geospatial approach employs variogram-based imputation to model spatial correlations between equipped and unequipped links, refining the traffic estimates. The output from both approaches generates an estimation of traffic variables across the whole network, incorporating data from both sensor-equipped links and estimated values for non-equipped links. Figure 1 represents an overview of the proposed methodologies in a flowchart.

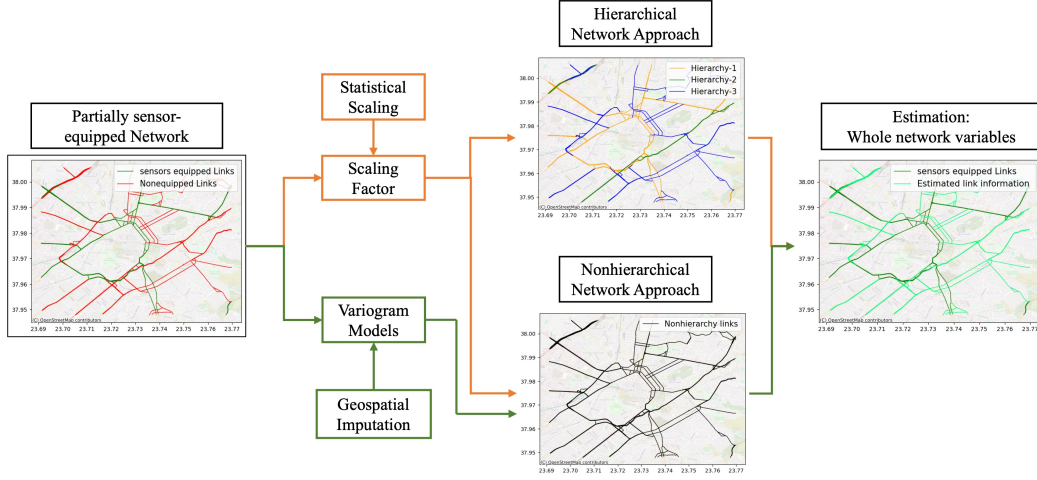


Figure 1: An overview of the overall methodology for estimating whole network variables from the partially-equipped network

3.1. Statical Scaling

Let's assume a traffic network (Ω), having links (i) of n numbers, with a different hierarchy based on serviceability, defined as link class as t . Among all the links, some have loop detectors (LDs) count as j . Therefore, the flow in the links of LDs can be presented as $\{q_j \mid j \in i\}$. The overall network flow (q_N) and LDs equipped network flow (q_{eq}) can be expressed by total travel distance (TTD) as network 'production' by all vehicles over the time-space region, shown as follows:

$$\bar{q}_{eq} = \frac{\sum_{\forall t} TTD_{eq}}{\sum_{\forall j,t} l_{j,t} \Delta t} \quad (1a)$$

$$= \frac{\sum_{\forall j,t} q_{j,t} l_{j,t}}{\sum_{\forall j,t} l_{j,t}} \quad (1b)$$

$$\bar{q}_N = \frac{\sum_{\forall t} TTD}{\sum_{\forall i,t} l_{i,t} \Delta t} \quad (1c)$$

$$= \frac{\sum_{\forall t} TTD_{eq} + \sum_{\forall t} TTD_{neq}}{\sum_{\forall i,t} l_{i,t} \Delta t} \quad (1d)$$

$$\sum_{\forall t} TTD_{eq} = \sum_{\forall j,t} q_{j,t} l_{j,t} \quad (2)$$

$$\mathbb{E}(q_{j,t} l_{j,t}) = \mathbb{E}(q_{j,t}) \mathbb{E}(l_{j,t}) + Cov(q_{j,t}, l_{j,t}) \quad (3)$$

$$\frac{1}{m} \sum_{\forall t} \sum_{j=1}^m q_{j,t} l_{j,t} = \sum_{\forall t} \left(\frac{1}{m} \sum_{j=1}^m q_{j,t} \right) \frac{1}{m} \sum_{\forall t} \sum_{j=1}^m l_{j,t} + Cov(q_{j,t}, l_{j,t}) \quad (4)$$

$$\sum_{\forall j,t} q_{j,t} l_{j,t} = \sum_{\forall t} (\bar{q}_{eq,t}) \sum_{\forall j,t} l_{j,t} + m \times Cov(q_{j,t}, l_{j,t}) \quad (5)$$

Similarly, for not equipped network:

$$\sum_{\forall t} TTD_{neq} = \sum_{\forall i \notin j,t} q_{i,t} l_{i,t} \quad (6)$$

$$\mathbb{E}(q_{i,t} l_{i,t} | \forall i \notin j, t) = \mathbb{E}(q_{i,t} | \forall i \notin j, t) \mathbb{E}(l_{i,t} | \forall i \notin j, t) + Cov(q_{i,t} l_{i,t} | \forall i \notin j, t) \quad (7)$$

$$\sum_{\forall t} \sum_{i=1}^n q_{i,t} l_{i,t} = \sum_{\forall t} (\bar{q}_{neq,t}) \sum_{\forall t} \sum_{i=1}^n l_{i,t} + Cov(q_{i,t} l_{i,t} | \forall i \notin j, t) \quad (8)$$

$$\sum_{\forall i \notin j,t} q_{i,t} l_{i,t} = \sum_{\forall t} (\bar{q}_{neq,t}) \sum_{\forall i \notin j,t} l_{i,t} + n \times Cov(q_{i,t} l_{i,t} | \forall i \notin j, t) \quad (9)$$

Assuming the mean flow and covariance of flow for a unique link hierarchy will be the same. Therefore,

$$\bar{q}_{neq,t} = \bar{q}_{eq,t}, Cov(q_{j,t}, l_{j,t}) = Cov(q_{i,t} l_{i,t} | \forall i \notin j, t) \quad (10)$$

$$\sum_{\forall i \notin j,t} q_{i,t} l_{i,t} = \frac{\sum_{\forall j,t} q_{j,t} l_{j,t}}{\sum_{\forall j,t} l_{j,t}} \sum_{\forall i \notin j,t} l_{i,t} + n \times Cov(q_{j,t}, l_{j,t}) \quad (11)$$

$$= \sum_{\forall j,t} q_{j,t} l_{j,t} \frac{\sum_{\forall i \notin j,t} l_{i,t}}{\sum_{\forall j,t} l_{j,t}} + n \times Cov(q_{j,t}, l_{j,t}) \quad (12)$$

Thus, the total network flow can be formulated from the equipped network

information as follows:

$$\hat{q} = \frac{\sum_{\forall t} TTD}{\sum_{\forall i,t} l_{i,t} \Delta t} \quad (13)$$

$$= \frac{\sum_{\forall t} TTD_{eq} + \sum_{\forall t} TTD_{neq}}{\sum_{\forall i,t} l_{i,t} \Delta t} \quad (14)$$

$$= \frac{\sum_{\forall j,t} q_{j,t} l_{j,t} + (\sum_{\forall j,t} q_{j,t} l_{j,t} \frac{\sum_{\forall i \notin j,t} l_{i,t}}{\sum_{\forall j,t} l_{j,t}} + n \times Cov(q_{j,t}, l_{j,t}))}{\sum_{\forall i,t} l_{i,t} \Delta t} \quad (15)$$

Similarly, we can derive the network average density from the equipped network information. The network average density can be expressed by total travel time (TTT) as the ‘accumulation’ spent by all vehicles in the network over the time-space domain.

$$\hat{k} = \frac{\sum_{\forall t} TTT}{\sum_{\forall i,t} l_{i,t} \Delta t} \quad (16)$$

$$= \frac{\sum_{\forall t} TTT_{eq} + \sum_{\forall t} TTT_{neq}}{\sum_{\forall i,t} l_{i,t} \Delta t} \quad (17)$$

$$= \frac{\sum_{\forall j,t} k_{j,t} l_{j,t} + (\sum_{\forall j,t} k_{j,t} l_{j,t} \frac{\sum_{\forall i \notin j,t} l_{i,t}}{\sum_{\forall j,t} l_{j,t}} + n \times Cov(k_{j,t}, l_{j,t}))}{\sum_{\forall i,t} l_{i,t} \Delta t} \quad (18)$$

The q_j and k_j are the flow and density in the detector level in a link.

3.2. Geo-spatial Scaling: variogram

Kriging is a well-established geostatistical interpolation method initially developed by Krige [68] and later expanded by Matheron [69]. It has been applied across various disciplines for spatial data interpolation, including missing data imputation in traffic studies. The central component of kriging is the variogram, a function that models the spatial correlation between data points. The variogram provides an essential representation of how spatial dependence changes with distance, guiding Kriging’s ability to estimate unknown values at unobserved locations based on nearby known observations [70].

Variogram models, such as spherical, exponential, and Gaussian models, are typically fitted to the empirical variogram to quantify spatial continuity

[71]. These models help define the structure of spatial relationships and enable kriging to make predictions.

3.2.1. Spatial Dependency and Variogram

Let the traffic flow data for certain links in a network be given as $\{(s_i, q_i)\}$, where $s_i = (x_i, y_i)$ represents the geographical coordinates (latitude and longitude) of the i -th known link, and q_i is the observed traffic flow at that link. The task is to estimate traffic flow $q(s_0)$ at unknown locations s_0 by leveraging spatial interpolation techniques based on kriging and a variogram model.

The variogram measures the spatial dependence of a random variable, in this case, traffic flow, across a network. The variogram $\gamma(h)$ represents how traffic flow differences are expected to change with increasing distance (h) between two locations. Unlike the traditional variogram model's spatial distance, in this study, the distance between two locations is measured by the shortest path distance. For any two points s_i and s_j separated by distance $h = \|s_i - s_j\|$, the variogram is defined as:

$$\gamma(h) = \frac{1}{2} \mathbb{E} [(q(s_i) - q(s_j))^2] \quad (19)$$

Here, \mathbb{E} denotes the expectation, and h is the shortest path distance between s_i and s_j .

The variogram is often approximated from data using the empirical variogram:

$$\gamma(h) = \frac{1}{2N(h)} \sum_{s_i, s_j: \|s_i - s_j\|=h} (q_i - q_j)^2 \quad (20)$$

where $N(h)$ is the number of pairs of points separated by distance h . This empirical variogram helps identify the spatial structure in the traffic flow data. The variogram $\gamma(h)$ is typically modeled using one of several functional forms (e.g., spherical, exponential, Gaussian) based on the empirical semivariances derived from the data. For instance, the spherical variogram is expressed as:

$$\gamma(r) = \begin{cases} C_0 + C \left(\frac{3r}{2a} - \frac{r^3}{2a^3} \right), & \text{if } r \leq a \\ C_0 + C, & \text{if } r > a \end{cases} \quad (21)$$

where a is the range, C_0 is the nugget, and C is the sill, serve as constants

for the model.

3.2.2. Spatial Interpolation: Kriging System Setup

Once the variogram model is fitted, the traffic flow at unmeasured locations can be estimated using *Ordinary Kriging*. In Ordinary Kriging (OK) for traffic flow estimation, we aim to predict the traffic flow $\hat{q}(s_0)$ at an unmeasured location s_0 , using a weighted linear combination of the traffic flows $q(s_i)$ at known locations s_i , where $i = 1, 2, \dots, n$. The primary assumption in ordinary kriging is that the mean traffic flow $\bar{q}(s)$ is constant within a neighborhood of the target point s_0 . The following assumptions are considered:

- The deterministic component $\bar{q}(s)$, representing the mean traffic flow, is approximately constant across the neighborhood of interest, so $\bar{q}(s_0) \approx \bar{q}(s_i) \equiv \bar{q}$.
- The stochastic component $\epsilon(s)$, representing random fluctuations in traffic flow, is Gaussian-distributed with zero mean, and the correlation between flows at different locations depends on their spatial separation.

3.2.3. Ordinary Kriging Estimator:

The predicted traffic flow $\hat{q}(s_0)$ at location s_0 is given by:

$$\hat{q}(s_0) = \bar{q}(s_0) + \epsilon(s_0) \quad (22)$$

The random component can be defined as a weighted multiplication of the deviation of the observed traffic flow at s_i from the mean s_0 . The kriging weights w_i are applied to these deviations, meaning that locations closer to s_0 (with higher spatial correlation) will have a greater influence on the prediction. This spatially weighted adjustment ensures that the predicted traffic flow at s_0 not only considers the global mean \bar{q} but also incorporates the local variations (the deviations from the mean) based on the observed traffic flows at the nearby locations.

$$\hat{q}(s_0) = \bar{q} + \sum_{i=1}^n w_i (q(s_i) - \bar{q}) \quad (23)$$

Since \bar{q} is assumed to be constant, the estimator simplifies to:

$$\hat{q}(s_0) = \sum_{i=1}^n w_i q(s_i) + \bar{q} \left(1 - \sum_{i=1}^n w_i \right) \quad (24)$$

For an unbiased estimator, the weights w_i must satisfy the constraint:

$$\sum_{i=1}^n w_i = 1 \quad (25)$$

Therefore, the predicted traffic flow at s_0 is given by:

$$\hat{q}(s_0) = \sum_{i=1}^n w_i q(s_i) \quad (26)$$

This completes the estimation procedure for ordinary kriging, where the prediction of traffic flow at a target point is a weighted sum of the flows from nearby measured locations, with weights optimized to minimize prediction error while ensuring the estimator remains unbiased. This ensures that the expected value of the predicted traffic flow is equal to the expected value of the true traffic flow:

$$\mathbb{E} [\hat{q}(s_0)] = \bar{q} = \mathbb{E} [q(s_0)] \quad (27)$$

The kriging weights w_i are determined by solving the kriging system of $n + 1$ equations for the weights w_i and Lagrange multiplier μ is:

$$\begin{pmatrix} \gamma_{11} & \gamma_{12} & \dots & \gamma_{1n} & 1 \\ \gamma_{21} & \gamma_{22} & \dots & \gamma_{2n} & 1 \\ \vdots & \vdots & \ddots & \vdots & \vdots \\ \gamma_{n1} & \gamma_{n2} & \dots & \gamma_{nn} & 1 \\ 1 & 1 & \dots & 1 & 0 \end{pmatrix} \begin{pmatrix} w_1 \\ w_2 \\ \vdots \\ w_n \\ \mu \end{pmatrix} = \begin{pmatrix} \gamma_{10} \\ \gamma_{20} \\ \vdots \\ \gamma_{n0} \\ 1 \end{pmatrix} \quad (28)$$

Where γ_{ij} is the semivariance between known points s_i and s_j , γ_{i0} represents the semivariance between s_i and s_0 .

The next section describes the empirical data used in this study, focusing on LDD collected under varying levels of sensor deployment. Additionally, it outlines the link hierarchy classification, which forms the basis for the hierarchical scaling methodology proposed in this study.

4. Data

4.1. Data Description

The study focuses on the road network of downtown Athens, Greece, covering an area of approximately 40 km². The network, excluding minor roads, extends over 150 km in total length. The major roads, characterized by more than two lanes and a peak-hour traffic flow exceeding 1000 vehicles per lane per hour, are identified as the most important and busiest routes within the network. The data for this study was collected from loop detectors over a weekday period from November 7th to 11th, 2022, covering a 24-hour time span each day. The loop detector data provides location-based traffic information, such as traffic counts and average speeds.

The links in the road network were classified in two ways. The first classification follows a three-hierarchy (3-H), where roads are categorized into three groups: Link-1, the most critical roads, and Link-3, the least important major roads. The second classification follows a two-tier hierarchy (2-H), where the network is divided into two types: Link-1, representing the most important roads, and Link-2, which includes the remaining major roads. Notably, Link-1 is identical in both classifications, while Link-2 in the 2-H classification corresponds to Link-2 and Link-3 in the 3-H classification based on their average speeds and flow profiles. Figures 2 and 3 illustrate the comparison of average speeds and flow profiles for the 2-H and 3-H classifications.

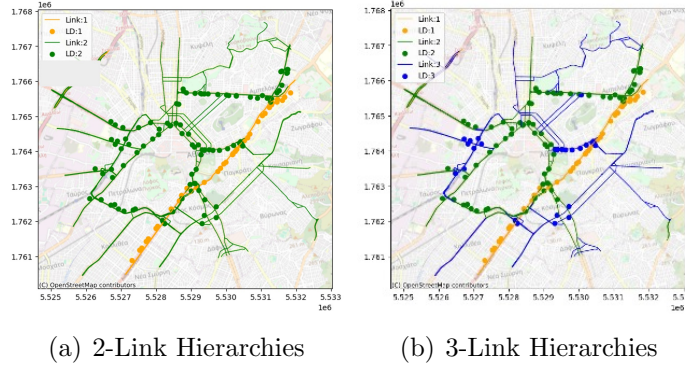


Figure 2: Network fully equipped with LDD and features hierarchical links, including (a) two types link, (b) three types link

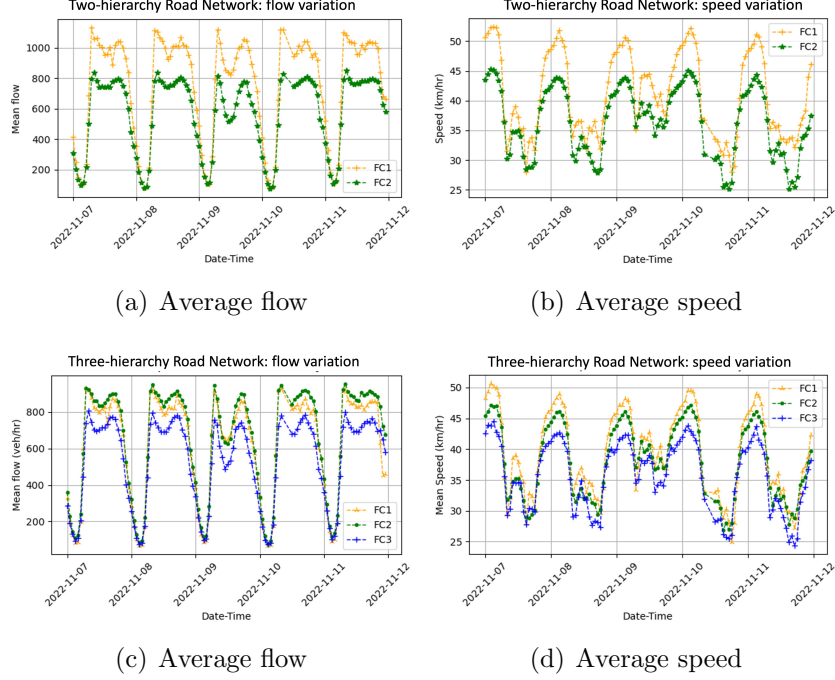
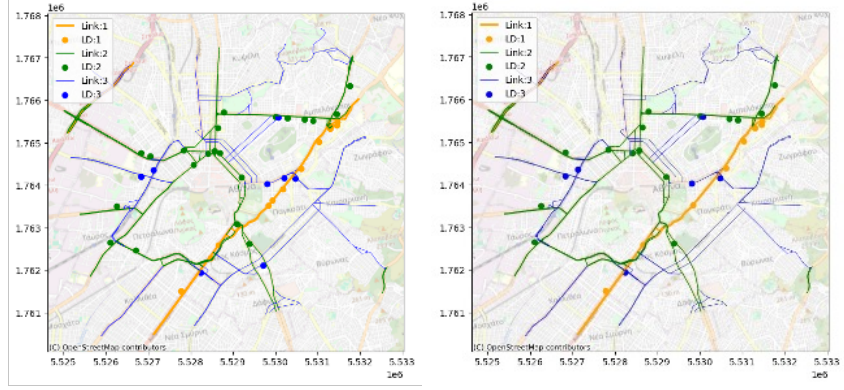


Figure 3: Comparison of average network flow ((a) two-hierarchy, (c) three-hierarchy) and speed ((b) two-hierarchy, (d) three-hierarchy) for different network configurations.

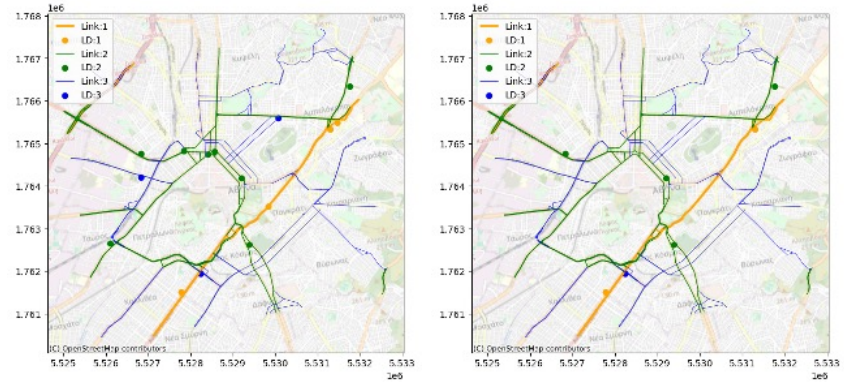
The entire network consists of 142 links, spanning different hierarchical levels within the 150 km network. A fully equipped network is defined as one in which all links have at least one LD. In this study, we considered the fully equipped network, which includes 142 LDs distributed across 142 links, as shown in Figures 2 (a, b). To evaluate our methodology, we also created partially equipped networks by randomly removing LDs from various links equally from each hierarchy in both the 2-H and 3-H hierarchical networks. Table 1 provides details on the number of LDs in each link type for the fully equipped (100%) network as well as for networks with 30%, 20%, 10%, and 5% LD coverage. Figure 4 illustrates the distribution of LDs in these partially equipped networks.

In this study, we validated our approach using three different network types: the 2-H network, the 3-H network, and a non-hierarchical network.



(a) 30% LD of Figure 1 network

(b) 20% LD of Figure 1 network



(c) 10% LD of Figure 1 network

(d) 05% LD of Figure 1 network

Figure 4: Partially loop detectors equipped networks (a) 30% LD equipped network, (b) 20% LD equipped network, (c) 10% LD equipped network, and (d) 05 % LD equipped network

Table 1: Description of loop detector-equipped link in the fully equipped and partially equipped network

Equipped Network (% LD)	3-Hierarchies			2-Hierarchies		Non-Hierarchy
	Link-1	Link-2	Link-3	Link-1	Link-2	Link-all
100	39 (20 km)	75 (60 km)	28 (70 km)	45 (20 km)	95 (130 km)	142 (150 km)
30	12	22	8	16	26	42
20	8	15	6	10	19	29
10	4	8	3	6	9	15
5	2	4	1	3	4	7

Next, section 5 presents the results of applying these methodologies, focusing on the estimation of network demand and MFDs. A comparative analysis of all proposed methods is provided, highlighting their performance under varying levels of sensor deployment.

5. Results

In this section, we discuss the flow estimation for the whole network from equipped network information. The study proposes two methods: first, statistical scaling of the equipped network and application to the different hierarchical structures of the network. In this study, we demonstrate a two-hierarchical, three-hierarchical, and non-hierarchical network approach to applying the proposed scaling method. Second, the variogram method of spatial scaling, where the empirical variogram calibrates the spherical variogram model using flow distribution in the equipped network and spatially interpolates the flow in the full network. Since the variogram model was developed based on geospatial scaling, we only apply this method to a non-hierarchical network approach.

5.1. Flow Estimation using Geo-spatial methods: variogram

The Variogram model takes input of flow from the equipped network's links and estimates flow spatially over the full network. Figure 5 demonstrates the flow estimation spatially with respect to different percentages of LD-equipped networks at various times of the day. The color-coded flow plots

visually represent traffic flow intensity across the network links, with the gradient indicating varying flow levels, from low (blue) to high (red). Since this study focuses on flow scaling only on the major roads (Link-1, link-2, link-3), we only extracted information along the links in the major roads. The first column of Figure 5, where 30% of the network’s major links are equipped with loop detectors (LD), the Variogram model produces a detailed and accurate estimation of flow across all major and minor links. Congestion hotspots, as indicated by red zones, align closely with expected traffic patterns, validating the model’s capability to capture traffic dynamics effectively under sufficient LD coverage. As the LD percentage is reduced to 20% and 10%, shown in the subsequent columns, the model maintains a good estimation quality of the overall network flow, with significant flow details retained for major road links (Link-1, Link-2, and Link-3). Congestion hotspots and the broader distribution of flow are generally well-captured, indicating the robustness of the Variogram-based estimation even under reduced LD coverage.

When we reduced LD percentage by 20 %, 10% as per Table 1, we could see that the model can estimate the whole network flow along with the major link networks perfectly with the matching of congestion hotspots and other traffic conditions mostly over the different time of the day. As we further decrease the LD percentage to 5%, this method could not able to estimate full network traffic flow because of the sparse information with respect to the variogram radius of estimation. Therefore, this method is best suited for network flow scaling of an equipped network having more than 10 % LD. However, at the 5% LD level (final column), the model’s performance declines. Sparse detector data creates spatial gaps that hinder accurate network flow estimation. This results in less precise representations of flow across the network, with notable discrepancies in congestion hotspots and overall flow intensity. This limitation highlights the importance of maintaining a critical mass of LD coverage for accurate spatial flow estimation.

Across all LD percentages, flow estimations vary consistently throughout the day (from 08:00 to 17:00). Peak traffic hours show distinct congestion patterns, emphasizing the model’s sensitivity to temporal variations in traffic demand and conditions. The consistent ability of the Variogram model to capture these temporal patterns, even as LD coverage changes, is a notable strength. This analysis underscores that the Variogram-based method for network flow scaling performs optimally with LD coverage of at least 10%. Below this threshold, estimation accuracy declines significantly due to sparse spatial data, reducing the reliability of flow predictions.

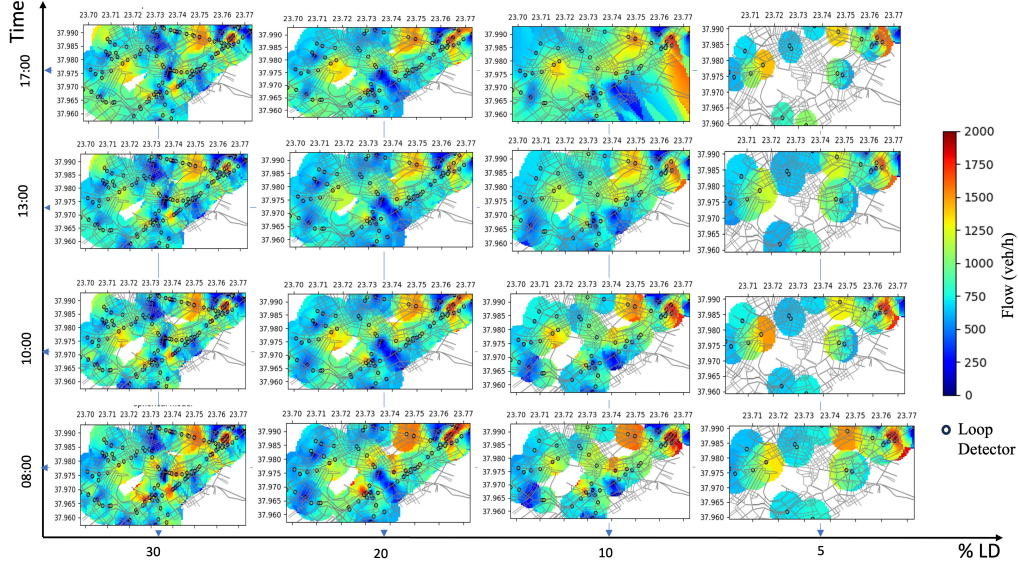


Figure 5: Traffic flow prediction from the equipped network to the entire network using the Variogram method. The x-axis represents the equipped network with varying LD percentages, while the y-axis depicts traffic flow at different hours of the day at both the LD position and network level.

5.2. Comparison of proposed methods

The results in Figure 6 and Figure 7, combined with the RMSE values presented in Table 2, provide insight into the comparative performance of the proposed statistical (non-hierarchical, 2-hierarchy (2-H), 3-hierarchy (3-H)) and the variogram methods (non-hierarchical) for estimating network flow under different LD coverage percentages (5%, 10%, 20%, and 30%). The temporal flow estimations in Figure 6 demonstrate that higher LD coverage leads to more accurate flow predictions across all methods. This trend is further supported by the RMSE values, which generally decrease as LD coverage increases, especially for the hierarchical and Variogram methods.

At the lowest LD coverage (5%), the Variogram method is unable to estimate flow across the entire network, reflecting a limitation in this approach when LD coverage falls below 10%. Meanwhile, the remaining methods, particularly the 3-Hierarchy, continue to provide estimations, though with elevated RMSE values (e.g., RMSE of 65-64 on day 1 and day 4 for the 3-Hierarchy method). This highlights the robustness of hierarchical frameworks compared to geospatial estimation techniques like the Variogram, which re-

quire a minimum density of LDs for effective network-wide prediction. At 10% LD coverage, the Variogram method becomes viable and achieves relatively low RMSE values compared to non-hierarchical methods, indicating an improvement in estimation accuracy with increased LD density. Across all methods, higher LD coverage continues to yield more accurate predictions, with RMSE values substantially decreasing by the time LD coverage reaches 30%. Here, both the 3-Hierarchy and Variogram methods achieve RMSE values close to or below 15, showcasing their potential for precise flow estimation even with partial network monitoring. In the statistical methods, increasing the number of hierarchical levels in the network consistently enhances estimation accuracy. For any given LD coverage percentage, the 3-hierarchy (3-H) network consistently outperforms both the 2-hierarchy (2-H) and non-hierarchical approaches.

The scatter plots in Figure 7 further illustrate these trends, showing the spread of estimated flow values relative to actual flow values from a fully equipped network. As LD coverage decreases, the spread around the ideal $x = y$ line widens, particularly for the non-hierarchical method, which exhibits greater deviations from actual values. Conversely, the 3-Hierarchy and variogram approaches demonstrate tighter clustering around the ideal line, especially at lower LD coverages, reaffirming their superior accuracy under moderate to high LD densities.

These results underscore the robustness of hierarchical models, particularly in sparse LD conditions where unstructured methods like the Variogram may falter. The 3-Hierarchy method, in particular, shows resilience across all coverage levels, while the Variogram method performs strongly at 10% and higher LD coverage, demonstrating its potential for accurate network-wide estimations when sufficient spatial data is available. The non-hierarchical approach, while less accurate, serves as a baseline, illustrating the limitations of unstructured models in low-coverage scenarios. Overall, these findings underscore the value of incorporating hierarchical and spatially structured models to enhance traffic flow estimations in partially monitored networks.

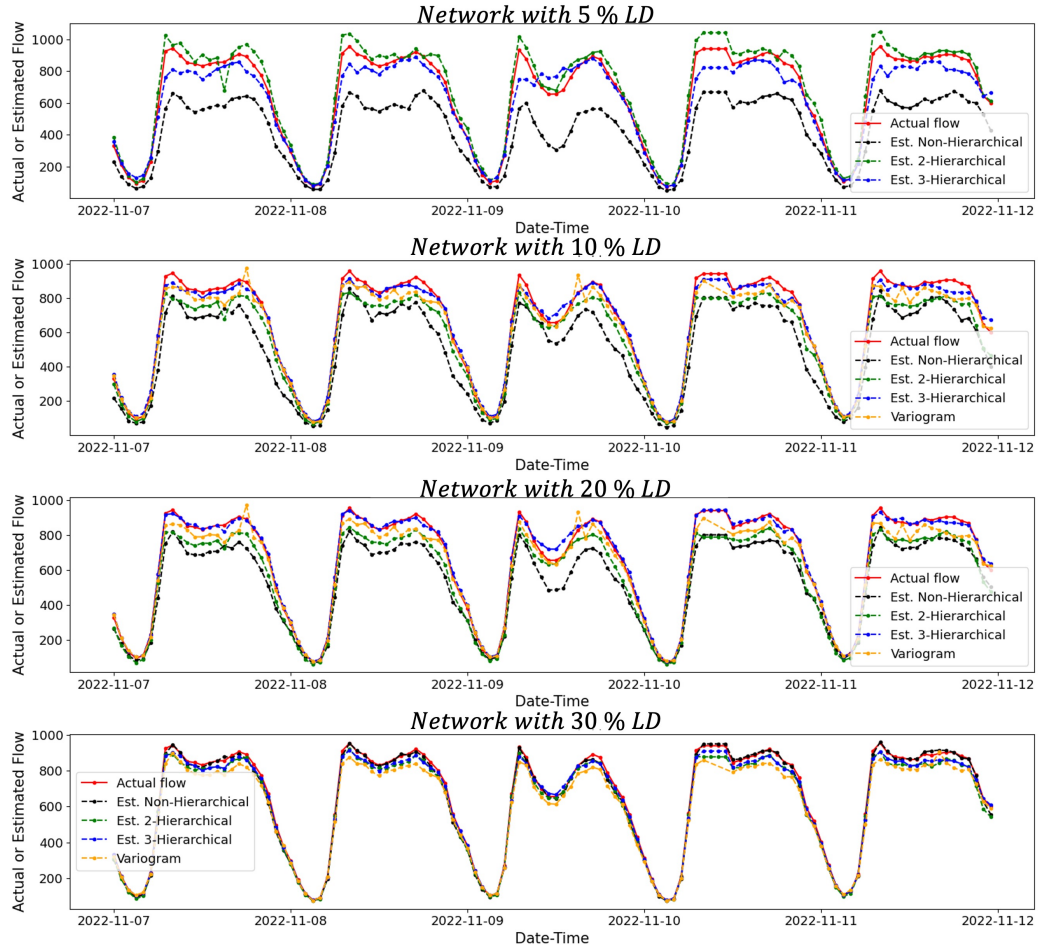


Figure 6: Comparisons of estimated hourly network flow using different methods with different loop detector equipped network level.

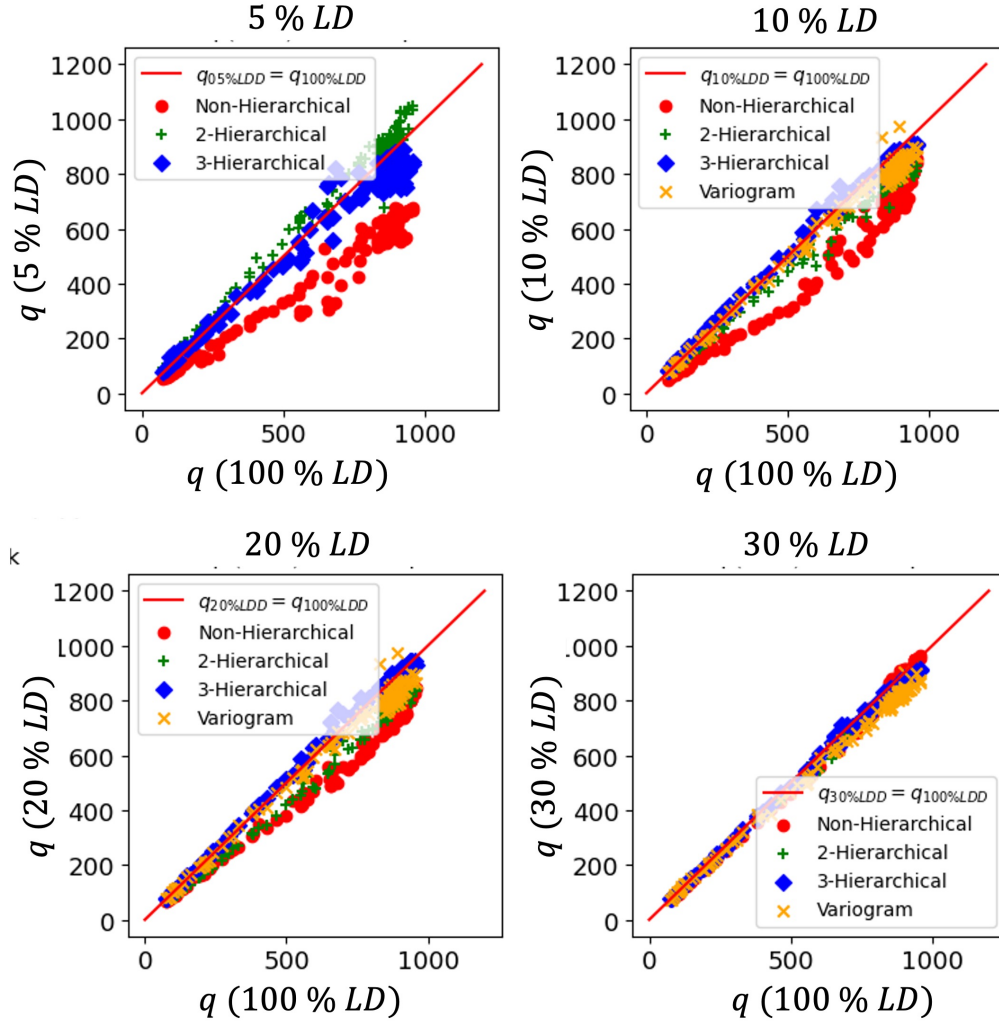


Figure 7: Comparison of actual network flow based on fully equipped network information (100% LD) with estimated flow derived from a partially equipped network. The x-axis represents the actual flow, while the y-axis denotes the estimated flow. From left to right, the subfigures illustrate comparisons for 5%, 10%, 20%, and 30% LD.

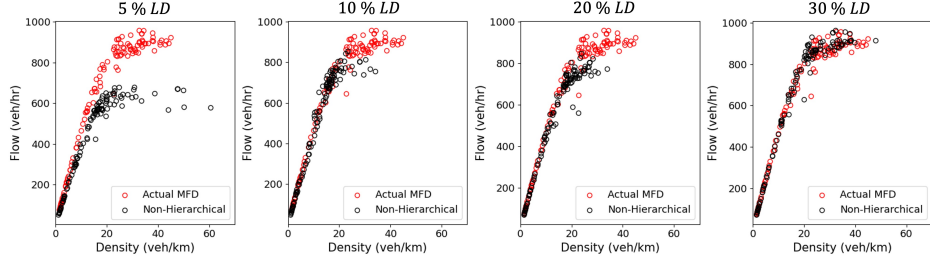
Table 2: Comparison of root mean square error (RMSE) of network flow, estimated using different network scaling methods

Day	Network (% LD)	3-H	2-H	Non-hierarchy	Variogram
day1	30	12	30	24	12
	20	12	85	128	17
	10	26	90	158	43
	5	65	110	226	-
day2	30	13	29	20	15
	20	14	83	127	29
	10	26	87	148	45
	5	53	108	232	-
day3	30	25	24	20	42
	20	27	70	133	27
	10	28	83	142	42
	5	51	120	260	-
day4	30	12	37	17	25
	20	13	94	119	15
	10	31	98	144	39
	5	64	117	224	-
day5	30	13	42	16	31
	20	16	94	110	34
	10	35	95	145	39
	5	48	115	229	-

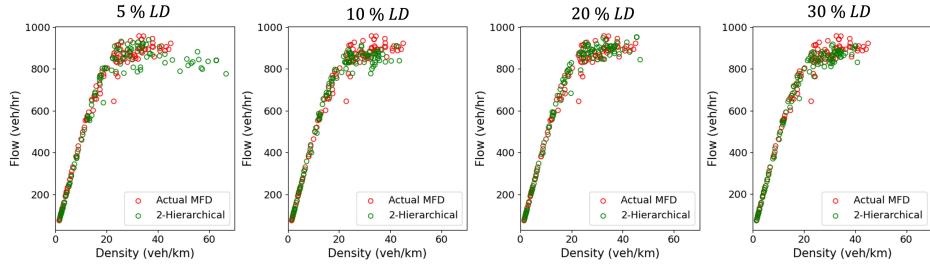
5.3. Comparing MFDs

This section demonstrates network MFDs estimated from the partially equipped network using the proposed scaling methodologies and compares them with the actual MFDs from the fully equipped network. In section 3.1, we proposed the network flow (\hat{q}) and density (\hat{k}) using the statistical scaling method, and section 3.2 described \hat{q} estimation using the variogram. Similarly, we can estimate \hat{k} using variogram methods by estimating detector-level density.

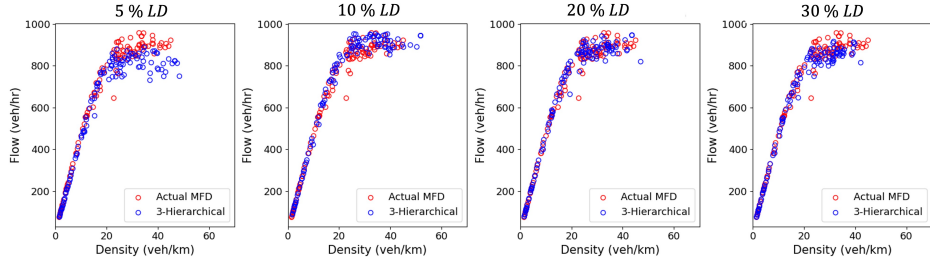
The estimated macroscopic fundamental diagrams (MFDs) derived from the proposed methodologies across varying LD coverage percentages demonstrate clear differences in accuracy among the methods employed, as summarized in Figure 8 and Table 3. The 5% LD scenario represents the most challenging condition for flow estimation due to sparse detector data. Among the methods, the three-hierarchy (3-H) statistical scaling achieves the lowest root mean square error (RMSE) of 48.9 veh/h, significantly outperforming the two-hierarchy (2-H) scaling (51.8 veh/h) and the non-hierarchical approach (175.5 veh/h). The high coefficient of determination ($R^2 = 0.97$) for the 3-H method further highlights its robustness in low-data scenarios, maintaining strong alignment with the actual MFD. For 10% LD, the 3-H scaling method again delivers superior results with an RMSE of 45.3 veh/h, slightly better than the 2-H method (45.7 veh/h), variogram (55.2 veh/h), and markedly better than the non-hierarchical approach (137.6 veh/h). At 20% LD, the differences between the hierarchical methods narrow further, with 3-H achieving 36.5 veh/h RMSE compared to 37.3 veh/h for 2-H. Both methods significantly outperform the non-hierarchical method (133.5 veh/h), demonstrating the effectiveness of incorporating spatial structure in flow estimation. At the highest detector coverage of 30%, all methods perform well due to the availability of more extensive data. However, the 3-H method remains the most accurate, with an RMSE of 35.9 veh/h, compared to 37.1 veh/h for 2-H and 39.9 veh/h for the non-hierarchical method. The variogram method also performs well in this scenario, achieving an RMSE of 51.5 veh/h, though its application is limited to LD coverage of 10% or greater.



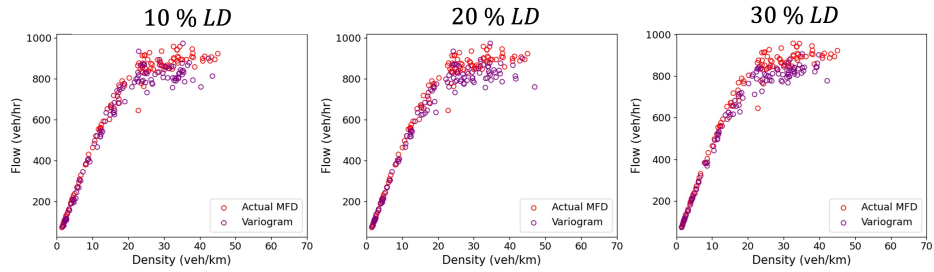
(a) Statistical scaling in non-hierarchical network



(b) Statistical scaling in two-hierarchical network



(c) Statistical scaling in three-hierarchical network



(d) Variogram scaling in non-hierarchical network

Figure 8: Comparison of estimated MFDs from partially equipped networks: (a, b, c) represent 5%, 10%, 20%, and 30% LD from left to right, and (d) shows 10%, 20%, and 30% LD from left to right, compared with the actual MFD derived from a fully equipped (100% LD) network.

Table 3: Comparison of estimated and actual MFDs

Method	Network Types	% LD	RMSE (veh/h)	R^2
Statistical	Non-hierarchy	30	39.9	0.98
		20	133.5	0.79
		10	137.6	0.78
		5	175.5	0.64
	Three-hierarchy	30	35.9	0.98
		20	36.5	0.98
		10	45.3	0.97
		5	48.9	0.97
	Two-hierarchy	30	37.1	0.98
		20	37.3	0.98
		10	45.7	0.97
		5	51.8	0.96
Variogram	Non-hierarchy	30	51.5	0.97
		20	54.6	0.96
		10	55.2	0.96

6. Discussion

The results underscore the critical role of hierarchical scaling in improving flow and MFD estimation accuracy, particularly under sparse data conditions. The 3-H method consistently outperforms the 2-H and non-hierarchical approaches across all LD levels, with its advantage most pronounced at low LD coverage (5% and 10%). This is likely due to the additional spatial structure incorporated in the 3-H scaling, which allows it to better capture localized variations in flow and density. At higher LD coverage (20% and 30%), the benefits of hierarchical approaches persist, though the performance gap between methods narrows. The non-hierarchical method shows improved accuracy as more data becomes available, but it remains less reliable than its hierarchical counterparts due to its inability to effectively extrapolate flow patterns in under-monitored regions. Interestingly, the variogram approach demonstrates competitive performance for LD coverage levels of 10% or more, but it cannot be applied at 5% LD due to insufficient data for spatial interpolation. This limitation highlights the trade-offs between different

methods in terms of data requirements and estimation capabilities. Overall, the findings emphasize the importance of leveraging hierarchical frameworks and structured statistical methods for MFD estimation, particularly in scenarios where data availability is limited. The superior performance of the 3-H method highlights its potential for practical applications in network flow analysis, even under challenging conditions. The insights gained from this study can inform future efforts to optimize traffic monitoring systems and enhance flow prediction accuracy.

7. Conclusion

This study presents a robust methodology for estimating network-wide traffic flow characteristics in partially sensor-equipped urban networks. By integrating statistical scaling and geospatial imputation techniques, the framework provides accurate estimations of macroscopic fundamental diagrams (MFDs), even in networks with sparse detector coverage. The hierarchical network approach, which categorizes links into three levels based on spatial and functional attributes, consistently outperforms non-hierarchical approaches, particularly at low levels of detector deployment (5%–10% LD). The results demonstrate that three-hierarchy statistical scaling achieves the lowest RMSE and highest R^2 values, highlighting its reliability for sparse sensor networks.

While the variogram-based geospatial method captures spatial correlations effectively, its limitations are evident in networks with very low detector density ($< 10\%LD$). As a geospatial interpolation tool, the variogram model estimates non-equipped link variables based on spatial distribution. Although route distances between links were used instead of Euclidean spatial distances, some interpolation errors may arise, affecting accuracy. In contrast, the statistical method is more promising because it assumes that links within the same hierarchy exhibit similar mean and covariance properties. However, challenges may emerge due to deviations in link characteristics, which can undermine the consistency of the scaling factors across different scenarios.

Despite these limitations, the proposed methodology offers a scalable and practical solution for estimating network-wide traffic conditions under varying levels of sensor availability. The findings underscore the potential of incorporating network structure and spatial dependencies in traffic modeling for real-world applications. This study bridges the gap between partial sen-

sor data and full-network traffic estimation, providing a scalable solution for cities with limited sensor coverage.

Acknowledgement

This research has received funding from the European Union’s Horizon Europe research and innovation program under Grant Agreement no. 101103808 (ACUMEN). The authors would like to thank Prof. Eleni I. Vlahogianni and her team from NTUA Athens for their support in providing traffic data.

References

- [1] C. F. Daganzo, N. Geroliminis, An analytical approximation for the macroscopic fundamental diagram of urban traffic, *Transportation Research Part B: Methodological* 42 (2008) 771–781. doi:10.1016/j.trb.2008.06.008.
- [2] M. Keyvan-Ekbatani, M. Yildirimoglu, N. Geroliminis, M. Papageorgiou, Multiple concentric gating traffic control in large-scale urban networks, *IEEE Transactions on Intelligent Transportation Systems* 16 (2015) 2141–2154. doi:10.1109/TITS.2015.2399303.
- [3] K. Ampountolas, N. Zheng, N. Geroliminis, Macroscopic modelling and robust control of bi-modal multi-region urban road networks, *Transportation Research Part B: Methodological* 104 (2017) 616–637. doi:10.1016/j.trb.2017.05.007.
- [4] K. Aboudolas, N. Geroliminis, Perimeter and boundary flow control in multi-reservoir heterogeneous networks, *Transportation Research Part B: Methodological* 55 (2013) 265–281. doi:10.1016/j.trb.2013.07.003.
- [5] G. Mariotte, L. Leclercq, Heterogeneous perimeter flow distributions and MFD-based traffic simulation, *Transportmetrica B* 7 (2019) 1378–1401. doi:10.1080/21680566.2019.1627954.
- [6] S. Jiang, M. Keyvan-Ekbatani, Hybrid perimeter control with real-time partitions in heterogeneous urban networks: An integration of deep learning and MPC, *Transportation Research Part C: Emerging Technologies* 154 (2023). doi:10.1016/j.trc.2023.104240.
- [7] C. Buisson, C. Ladier, Exploring the impact of homogeneity of traffic measurements on the existence of macroscopic fundamental diagrams, *Transportation Research Record* (2009) 127–136. doi:10.3141/2124-12.
- [8] N. Geroliminis, J. Sun, Hysteresis phenomena of a macroscopic fundamental diagram in freeway networks, in: *Procedia - Social and Behavioral Sciences*, volume 17, Elsevier Ltd, 2011, pp. 213–228. doi:10.1016/j.sbspro.2011.04.515.

- [9] M. Keyvan-Ekbatani, A. Kouvelas, I. Papamichail, M. Papageorgiou, Exploiting the fundamental diagram of urban networks for feedback-based gating, *Transportation Research Part B: Methodological* 46 (2012) 1393–1403. doi:10.1016/j.trb.2012.06.008.
- [10] M. Saberi, H. Mahmassani, Exploring properties of networkwide flow-density relations in a freeway network, *Transportation Research Record* (2012) 153–163. doi:10.3141/2315-16.
- [11] M. Keyvan-Ekbatani, M. Papageorgiou, I. Papamichail, Urban congestion gating control based on reduced operational network fundamental diagrams, *Transportation Research Part C: Emerging Technologies* 33 (2013) 74–87. doi:10.1016/j.trc.2013.04.010.
- [12] L. Ambühl, A. Loder, L. Leclercq, M. Menendez, Disentangling the city traffic rhythms: A longitudinal analysis of MFD patterns over a year, *Transportation Research Part C: Emerging Technologies* 126 (2021). doi:10.1016/j.trc.2021.103065.
- [13] G. Lee, Z. Ding, J. Laval, Effects of loop detector position on the macroscopic fundamental diagram, *Transportation Research Part C: Emerging Technologies* 154 (2023). doi:10.1016/j.trc.2023.104239.
- [14] O. Mousavizadeh, M. Keyvan-Ekbatani, On the important features for a well-shaped reduced network MFD estimation during network loading and recovery, *Transportation Research Part C: Emerging Technologies* 161 (2024). doi:10.1016/j.trc.2024.104539.
- [15] N. Geroliminis, C. F. Daganzo, Existence of urban-scale macroscopic fundamental diagrams: Some experimental findings, *Transportation Research Part B: Methodological* 42 (2008) 759–770. doi:10.1016/j.trb.2008.02.002.
- [16] V. V. Gayah, C. F. Daganzo, Clockwise hysteresis loops in the Macroscopic Fundamental Diagram: An effect of network instability, *Transportation Research Part B: Methodological* 45 (2011) 643–655. doi:10.1016/j.trb.2010.11.006.
- [17] N. Geroliminis, J. Sun, Properties of a well-defined macroscopic fundamental diagram for urban traffic, *Transportation Research Part*

- B: Methodological 45 (2011) 605–617. URL: <http://dx.doi.org/10.1016/j.trb.2010.11.004>. doi:10.1016/j.trb.2010.11.004.
- [18] H. Mahmassani, T. Hou, M. Saberi, Connecting networkwide travel time reliability and the network fundamental diagram of traffic flow, *Transportation Research Record* (2013) 80–91. doi:10.3141/2391-08.
 - [19] T. Tsubota, A. Bhaskar, E. Chung, Macroscopic Fundamental Diagram for Brisbane, Australia, *Transportation Research Record: Journal of the Transportation Research Board* 2421 (2014) 12–21. doi:10.3141/2421-02.
 - [20] L. Ambühl, M. Menendez, Data fusion algorithm for macroscopic fundamental diagram estimation, *Transportation Research Part C: Emerging Technologies* 71 (2016) 184–197. doi:10.1016/j.trc.2016.07.013.
 - [21] J. Yang Beibei, H. J. van Zuylen, L. Shoufeng, Determining the Macroscopic Fundamental Diagram on the Basis of Mixed and Incomplete Traffic Data, in: *TRB 2016 Annual Meeting*, 2016, pp. 1–13.
 - [22] J. Du, H. Rakha, V. V. Gayah, Deriving macroscopic fundamental diagrams from probe data: Issues and proposed solutions, *Transportation Research Part C: Emerging Technologies* 66 (2016) 136–149. doi:10.1016/j.trc.2015.08.015.
 - [23] M. Saeedmanesh, N. Geroliminis, Clustering of heterogeneous networks with directional flows based on "Snake" similarities, *Transportation Research Part B: Methodological* 91 (2016) 250–269. doi:10.1016/j.trb.2016.05.008.
 - [24] L. . Ambühl, A. . Loder, M. . Menendez, K. W. Axhausen, Empirical Macroscopic Fundamental Diagrams New insights from loop detector and floating car data (2017). URL: <https://doi.org/10.3929/ethz-b-000167171>. doi:10.3929/ethz-b-000167171.
 - [25] I. Dakic, M. Menendez, On the use of Lagrangian observations from public transport and probe vehicles to estimate car space-mean speeds in bi-modal urban networks, *Transportation Research Part C: Emerging Technologies* 91 (2018) 317–334. doi:10.1016/j.trc.2018.04.004.

- [26] G. Mariotte, L. Leclercq, S. F. Batista, J. Krug, M. Paipuri, Calibration and validation of multi-reservoir MFD models: A case study in Lyon, *Transportation Research Part B: Methodological* 136 (2020) 62–86. doi:10.1016/j.trb.2020.03.006.
- [27] G. Mariotte, M. Paipuri, L. Leclercq, Dynamics of Flow Merging and Diverging in MFD-Based Systems: Validation vs. Microsimulation, *Frontiers in Future Transportation* 1 (2020). doi:10.3389/ffutr.2020.604088.
- [28] L. Leclercq, N. Chiabaut, B. Trinquier, Macroscopic Fundamental Diagrams: A cross-comparison of estimation methods, *Transportation Research Part B: Methodological* 62 (2014) 1–12. URL: <http://dx.doi.org/10.1016/j.trb.2014.01.007>. doi:10.1016/j.trb.2014.01.007.
- [29] J. Shim, J. Yeo, S. Lee, S. H. Hamdar, K. Jang, Empirical evaluation of influential factors on bifurcation in macroscopic fundamental diagrams, *Transportation Research Part C: Emerging Technologies* 102 (2019) 509–520. doi:10.1016/j.trc.2019.03.005.
- [30] H. Fu, Y. Wang, X. Tang, N. Zheng, N. Geroliminis, Empirical analysis of large-scale multimodal traffic with multi-sensor data, *Transportation Research Part C: Emerging Technologies* 118 (2020). doi:10.1016/j.trc.2020.102725.
- [31] S. Jiang, M. Keyvan-Ekbatani, D. Ngoduy, Partitioning of urban networks with polycentric congestion pattern for traffic management policies: Identifying protected networks, *Computer-Aided Civil and Infrastructure Engineering* 38 (2023) 508–527. doi:10.1111/mice.12895.
- [32] M. Saeedmanesh, N. Geroliminis, Dynamic clustering and propagation of congestion in heterogeneously congested urban traffic networks, *Transportation Research Part B: Methodological* 105 (2017) 193–211. doi:10.1016/j.trb.2017.08.021.
- [33] Z. Gu, M. Saberi, A bi-partitioning approach to congestion pattern recognition in a congested monocentric city, *Transportation Research Part C: Emerging Technologies* 109 (2019) 305–320. doi:10.1016/j.trc.2019.10.016.

- [34] M. Johari, S. Jiang, M. Keyvan-Ekbatani, D. Ngoduy, Mode differentiation in partitioning of mixed bi-modal urban networks, *Transportmetrica B* 11 (2023) 463–485. doi:10.1080/21680566.2022.2089271.
- [35] L. C. EDIE, Discussion of traffic stream measurements and definitions, *The 2nd International Symposium on Theory of Traffic flow*, London. 105 (1963) 139–154.
- [36] M. Johari, M. Keyvan-Ekbatani, L. Leclercq, D. Ngoduy, H. S. Mahmassani, Macroscopic network-level traffic models: Bridging fifty years of development toward the next era, *Transportation Research Part C: Emerging Technologies* 131 (2021). doi:10.1016/j.trc.2021.103334.
- [37] N. Zheng, N. Geroliminis, On the distribution of urban road space for multimodal congested networks, *Transportation Research Part B: Methodological* 57 (2013) 326–341. doi:10.1016/j.trb.2013.06.003.
- [38] E. Saffari, M. Yildirimoglu, M. Hickman, A methodology for identifying critical links and estimating macroscopic fundamental diagram in large-scale urban networks, *Transportation Research Part C: Emerging Technologies* 119 (2020). doi:10.1016/j.trc.2020.102743.
- [39] T. Seo, A. M. Bayen, T. Kusakabe, Y. Asakura, Traffic state estimation on highway: A comprehensive survey, *Annual Reviews in Control* 43 (2017) 128–151. doi:10.1016/j.arcontrol.2017.03.005.
- [40] A. Takayasu, L. Leclercq, N. Geroliminis, Experimental assessment of traffic density estimation at link and network level with sparse data, *Transportmetrica B* 10 (2022) 368–395. doi:10.1080/21680566.2021.2002738.
- [41] X. Wu, H. X. Liu, N. Geroliminis, An empirical analysis on the arterial fundamental diagram, *Transportation Research Part B: Methodological* 45 (2011) 255–266. URL: <http://dx.doi.org/10.1016/j.trb.2010.06.003>. doi:10.1016/j.trb.2010.06.003.
- [42] A. Nantes, D. Ngoduy, A. Bhaskar, M. Miska, E. Chung, Real-time traffic state estimation in urban corridors from heterogeneous data, *Transportation Research Part C: Emerging Technologies* 66 (2016) 99–118. doi:10.1016/j.trc.2015.07.005.

- [43] N. Maiti, B. R. Chilukuri, Estimation of local traffic conditions using Wi-Fi sensor technology, *Journal of Intelligent Transportation Systems* 28 (2024) 618–635. doi:10.1080/15472450.2023.2177103.
- [44] Qing-Jie Kong, Zhipeng Li, Yikai Chen, Yuncai Liu, An Approach to Urban Traffic State Estimation by Fusing Multisource Information, *IEEE Transactions on Intelligent Transportation Systems* 10 (2009) 499–511. doi:10.1109/TITS.2009.2026308.
- [45] K. Anuar, F. Habtemichael, M. Cetin, Estimating Traffic Flow Rate on Freeways from Probe Vehicle Data and Fundamental Diagram, in: *2015 IEEE 18th International Conference on Intelligent Transportation Systems*, IEEE, 2015, pp. 2921–2926. doi:10.1109/ITSC.2015.468.
- [46] S. Lu, V. L. Knoop, M. Keyvan-Ekbatani, Using taxi GPS data for macroscopic traffic monitoring in large scale urban networks: Calibration and MFD derivation, in: *Transportation Research Procedia*, volume 34, Elsevier B.V., 2018, pp. 243–250. doi:10.1016/j.trpro.2018.11.038.
- [47] C. Chen, J. Kwon, J. Rice, A. Skabardonis, P. Varaiya, Detecting Errors and Imputing Missing Data for Single-Loop Surveillance Systems, *Transportation Research Record: Journal of the Transportation Research Board* 1855 (2003) 160–167. doi:10.3141/1855-20.
- [48] D. W. Xu, H. H. Dong, H. J. Li, L. M. Jia, Y. J. Feng, The estimation of road traffic states based on compressive sensing, *Transportmetrica B: Transport Dynamics* 3 (2015) 131–152. doi:10.1080/21680566.2014.963736.
- [49] K. J. Offor, L. Vaci, L. S. Mihaylova, Traffic Estimation for Large Urban Road Network with High Missing Data Ratio, *Sensors* 19 (2019) 2813. doi:10.3390/s19122813.
- [50] E. Rossi, H. Kenlay, M. I. Gorinova, B. P. Chamberlain, X. Dong, M. Bronstein, On the Unreasonable Effectiveness of Feature propagation in Learning on Graphs with Missing Node Features (2021). URL: <http://arxiv.org/abs/2111.12128>.

- [51] H. Taguchi, X. Liu, T. Murata, Graph convolutional networks for graphs containing missing features, *Future Generation Computer Systems* 117 (2021) 155–168. doi:10.1016/j.future.2020.11.016.
- [52] J. A. Castro-Correa, J. H. Giraldo, A. Mondal, M. Badiey, T. Bouwmans, F. D. Malliaros, Time-varying Signals Recovery via Graph Neural Networks (2023). URL: <http://arxiv.org/abs/2302.11313><http://dx.doi.org/10.1109/ICASSP49357.2023.10096168>. doi:10.1109/ICASSP49357.2023.10096168.
- [53] Y. Bao, J. Liu, Q. Shen, Y. Cao, W. Ding, Q. Shi, PKET-GCN: Prior knowledge enhanced time-varying graph convolution network for traffic flow prediction, *Information Sciences* 634 (2023) 359–381. doi:10.1016/j.ins.2023.03.093.
- [54] J. Zhang, C. Song, S. Cao, C. Zhang, FDST-GCN: A Fundamental Diagram based Spatiotemporal Graph Convolutional Network for expressway traffic forecasting, *Physica A: Statistical Mechanics and its Applications* 630 (2023). doi:10.1016/j.physa.2023.129173.
- [55] Y. Zhang, B. Chen, S. Wang, J. Cao, GCGAN: Generative Adversarial Nets with Graph CNN for Network-Scale Traffic Prediction, in: 19. International Joint Conference on Neural Networks. Budapest, Hungary., IEEE, 2019. URL: <http://www.ieee.org/publications>.
- [56] H. Zheng, X. Li, Y. Li, Z. Yan, T. Li, GCN-GAN: Integrating Graph Convolutional Network and Generative Adversarial Network for Traffic Flow Prediction, *IEEE Access* 10 (2022) 94051–94062. doi:10.1109/ACCESS.2022.3204036.
- [57] J. Zhang, S. Mao, L. Yang, W. Ma, S. Li, Z. Gao, Physics-informed deep learning for traffic state estimation based on the traffic flow model and computational graph method, *Information Fusion* 101 (2024). doi:10.1016/j.inffus.2023.101971.
- [58] M. Usama, R. Ma, J. Hart, M. Wojcik, Physics-Informed Neural Networks (PINNs)-Based Traffic State Estimation: An Application to Traffic Network, *Algorithms* 15 (2022). doi:10.3390/a15120447.
- [59] J. K. Eom, M. S. Park, T.-Y. Heo, L. F. Huntsinger, Improving the Prediction of Annual Average Daily Traffic for Nonfreeway Facilities

- by Applying a Spatial Statistical Method, *Transportation Research Record: Journal of the Transportation Research Board* 1968 (2006) 20–29. doi:10.1177/0361198106196800103.
- [60] X. Wang, K. M. Kockelman, Forecasting Network Data, *Transportation Research Record: Journal of the Transportation Research Board* 2105 (2009) 100–108. doi:10.3141/2105-13.
 - [61] H. Zou, Y. Yue, Q. Li, A. G. Yeh, An improved distance metric for the interpolation of link-based traffic data using kriging: a case study of a large-scale urban road network, *International Journal of Geographical Information Science* 26 (2012) 667–689. doi:10.1080/13658816.2011.609488.
 - [62] B. Selby, K. M. Kockelman, Spatial prediction of traffic levels in unmeasured locations: applications of universal kriging and geographically weighted regression, *Journal of Transport Geography* 29 (2013) 24–32. doi:10.1016/j.jtrangeo.2012.12.009.
 - [63] J. Yang, L. D. Han, P. B. Freeze, S.-M. Chin, H.-L. Hwang, Short-Term Freeway Speed Profiling Based on Longitudinal Spatiotemporal Dynamics, *Transportation Research Record: Journal of the Transportation Research Board* 2467 (2014) 62–72. doi:10.3141/2467-07.
 - [64] D. Marcotte, Cokriging with matlab, *Computers & Geosciences* 17 (1991) 1265–1280. doi:10.1016/0098-3004(91)90028-C.
 - [65] B. Shamo, E. Asa, J. Membah, Linear Spatial Interpolation and Analysis of Annual Average Daily Traffic Data, *Journal of Computing in Civil Engineering* 29 (2015). doi:10.1061/(asce)cp.1943-5487.0000281.
 - [66] B. Bae, H. Kim, H. Lim, Y. Liu, L. D. Han, P. B. Freeze, Missing data imputation for traffic flow speed using spatio-temporal cokriging, *Transportation Research Part C: Emerging Technologies* 88 (2018) 124–139. doi:10.1016/j.trc.2018.01.015.
 - [67] J. Laval, Traffic Flow as a Simple Fluid: Towards a Scaling Theory of Urban Congestion, *Transportation Research Record: Journal of the Transportation Research Board* (2023). doi:10.1177/03611981231179703.

- [68] D. Krige, A statistical approach to some basic mine valuation problems on the Witwatersrand, *Journal of the Southern African Institute of Mining and Metallurgy* 52 (1951).
- [69] G. Matheron, Principles of geostatistics, *Economic Geology* 58 (1963) 1246–1266. doi:10.2113/gsecongeo.58.8.1246.
- [70] N. CRESSIE, *Statistics for spatial data*, John Wiley, New York Publication country United States, 1993.
- [71] M. A. R. W. Oliver, *A tutorial guide to geostatistics: Computing and modelling variograms and kriging*, volume 113, Catena, 2014.